Joule

CellPress

Article

A Printable Organic Cathode Interlayer Enables over 13% Efficiency for 1-cm^2 Organic Solar Cells

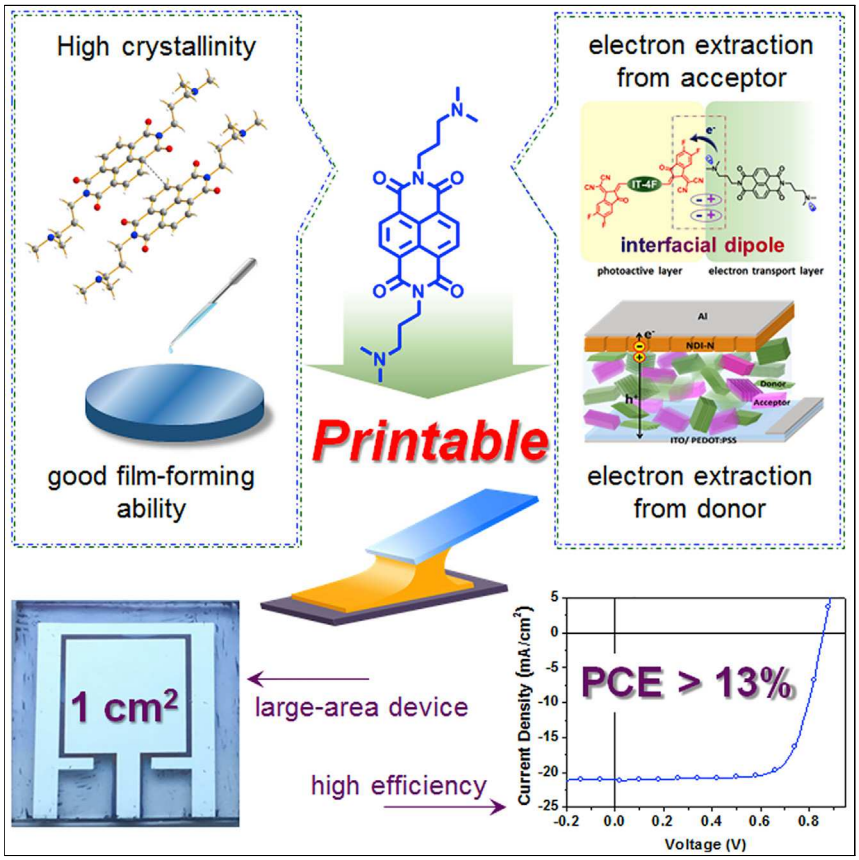

A naphthalene diimide (NDI)-based organic molecule (NDI-N) was prepared to be used as printable cathode interlayer (CIL) for organic solar cells (OSCs). NDI-N possesses combined advantages of high crystallinity and good film-forming properties, endowing the material with excellent electron-transport properties and good processability. NDI-N can be processed by printing methods; in this case an OSC device of 1 cm^2 was fabricated by using blade-coated NDI-N and an efficiency of 13.2% was achieved, which represents the highest efficiency to date for large-area OSCs.

Qian Kang, Long Ye, Bowei Xu, ..., Huifeng Yao, Harald Ade, Jianhui Hou

xubowei2004@iccas.ac.cn (B.X.)
hjhzlz@iccas.ac.cn (J.H.)

HIGHLIGHTS

A printable cathode interlayer (CIL) for OSCs is demonstrated for the first time

The high crystallinity and good processablity makes the organic CIL printable

The highest photovoltaic efficiency of large-area OSCs is achieved

Kang et al., Joule 3, 227–239
January 16, 2019
https://doi.org/10.1016/j.joule.2018.10.024

Joule

CellPress

Article

A Printable Organic Cathode Interlayer Enables over 13% Efficiency for 1-cm^2 Organic Solar Cells

Qian Kang,[1] Long Ye,[2] Bowei Xu,[1,*] Cunbin An,[1] Samuel J. Stuard,[2] Shaoqing Zhang,[1] Huifeng Yao,[1] Harald Ade,[2] and Jianhui Hou[1,3,*]

SUMMARY

Currently, most cathode interlayer (CIL) materials for organic solar cells (OSCs) cannot be processed by printing techniques, which severely limits their use in practical productions. Herein, we report a naphthalene diimide (NDI)-based small-molecular compound (*N*,*N*-dimethylamino)propyl naphthalene diimide (NDI-N) as printable CIL for OSCs. NDI-N exhibits a unique advantage that combines the merits of high crystallinity and good film-forming property in one material, endowing the semiconductor with excellent electron-transport properties and good processability. By using the NDI-N as CIL, a high power-conversion efficiency (PCE) of 13.9% was achieved in a PBDB-T-2F:IT-4F-based OSC device. More importantly, a large-area OSC device of 1 cm^2 was fabricated by using the blade-coated NDI-N CIL and an outstanding PCE of 13.2% was achieved, which represents the highest efficiency of large-area OSCs. The results in this work may pave the way for low-cost and mass production of OSCs.

INTRODUCTION

Organic solar cells (OSCs) have emerged as a promising renewable energy technology due to their advantages in fabricating lightweight and large-area devices through low-cost solution methods.[1–5] In the past two years the power-conversion efficiency (PCE) of OSCs has exceeded 14%, showing a bright prospect for practical applications.[6,7] At present, much attention focuses on manufacturing large-area OSCs by using printing techniques, believed to be crucial for the mass production.[8–10] So far, several photoactive materials as well as anode interlayer materials have been demonstrated to be processable by printing methods in fabricating efficient and large-area OSCs.[11,12] In contrast, owing to the low electron mobility, cathode interlayer (CIL) materials are very sensitive to the film thickness in modifying OSC devices, making them incompatible with large-area printing processes where certain thickness variation is unavoidable.[13–15] To date, only ZnO has been demonstrated as a successful example of a CIL that could be processed by a printing method in OSC fabrication.[16] Unfortunately, the PCE of the corresponding device was much lower than the efficiencies of state-of-the-art OSCs.[16] At present, the lack of printable CIL has greatly impeded the pace toward practical production of OSCs, and thus the development of a new CIL with high electron mobility is in urgent demand.

Among various *n*-type organic semiconductors, materials based on perylene diimide (PDI) and naphthalene diimide (NDI) show the most promising performance in OSCs due to their suitable energy levels and excellent electron-transport properties.[17–19]

Context & Scale

With the constantly enhanced photovoltaic efficiencies, as well as the advantages of low cost and light weight, organic solar cells (OSCs) exhibit a bright prospect for a new generation of renewable energy technology. For practical use, manufacturing large-area OSC devices by printing techniques is becoming critically important for the mass production of OSCs. However, the lack of printable cathode interlayer (CIL) materials has greatly impeded the pace toward practical production.

Here, we report an organic semiconductor possessing superior photoelectronic properties and good processablity, which is capable of serving as a printable CIL material. By using the printed CIL to make large-area devices, the highest photovoltaic efficiency for large-area OSCs was obtained, which paves the way for the commercialization and practical use of organic photovoltaics technology.

Compared with their PDI counterparts,[19,20] the NDI-based compounds possess higher optical transparency, making them more suitable in serving as charge-transport layer in OSCs.[21] Recently, a series of *n*-type self-doped conjugated polymers based on NDI were synthesized as CILs, and several outstanding PCEs were achieved in the OSCs by using the NDI-based CILs.[22,23] Due to the superior electron-transport properties, the NDI-based polymers exhibited an excellent thickness insensitivity in fabricating high-performance OSCs, implying their great potential for being processed by printing techniques.[24]

However, regarding molecular design, two conflicting factors between crystallinity and film-forming properties severely limits the development of NDI-based materials as printable CILs.[25] On the one hand, high crystallinity is essential to achieve superior charge-transport capacity for CILs, but the highly crystalline small molecules tend to aggregate during the film fabrication, resulting in a coarse film surface with pinholes;[26–28] this not only significantly deteriorates the device performance but also brings difficulties in processing CILs. On the other hand, NDI-based polymers exhibit improved film-forming properties; however, the low crystallinity and disordered molecular arrangement of polymers reduce their charge-transport capacity, restricting their further application in OSCs. To date these key problems have not been solved, thus limiting the use of NDI-based semiconductors for mass productions of OSCs. Although many reports demonstrate that a minor structural modification can drastically improve the performance of organic semiconductors,[29,30] it is still a great challenge to develop NDI-based compounds that combine the merits of high crystallinity and good film-forming properties.

Here we report an organic molecule based on naphthalene diimide, namely (*N*,*N*-dimethylamino)propyl naphthalene diimide (NDI-N), as a printable CIL for OSCs. NDI-N exhibits a unique advantage that combines the merits of high crystallinity and good film-forming properties in one material. By comparison of NDI-N and (*N*,*N*-dimethyl-*N*-ethylammonium)propyl naphthalene diimide (NDI-Br), an NDI-N analog modified with quaternary ammonium salt, it is found that NDI-N can efficiently extract electrons from both the non-fullerene acceptor and the polymer donor, which is superior to most currently used CILs. Using the NDI-N as CIL, OSCs with different photoactive layers all exhibit the best device performance in comparison with their highest values in related reports. More importantly, NDI-N can be processed by a printing method for making large-area devices; i.e., a large-area OSC device of 1 cm^2 was fabricated by using blade-coated NDI-N CIL and an outstanding PCE of 13.2% was achieved. To the best of our knowledge, this is the highest efficiency to date for large-area OSCs.

RESULTS AND DISCUSSION

The synthetic procedures of NDI-N and NDI-Br are illustrated in Figure 1A. NDI-N was prepared by a simple one-step reaction from commercially available compounds, 1,4,5,8-naphthalenetetracarboxylic dianhydride and *N*,*N*-dimethyl-1,3-propane-diamine, and was readily purified by recrystallization in ethanol, affording the lamellar crystal with a yield of 80%.[31] The ammonium-functionalized NDI-Br was synthesized by quaternizing the precursor compound NDI-N with excess bromoethane in *N*,*N*-dimethylformamide (DMF).[32] The molecular structures of NDI-N and NDI-Br were confirmed by ^{1}H nuclear magnetic resonance, MALDI-TOF with mass spectrometry, electrospray ionization mass spectrometry (Figure S1), and elemental analysis (Table S1). Both NDI-N and NDI-Br can be dissolved in polar organic solvents such as methanol, dimethylsulfoxide, and DMF. Figure 1B shows

[1]State Key Laboratory of Polymer Physics and Chemistry, Beijing National Laboratory for Molecular Sciences, Institute of Chemistry Chinese Academy of Sciences, Beijing 100190, P.R. China

[2]Department of Physics Organic and Carbon Electronics Lab (ORaCEL), North Carolina State University, Raleigh, NC 27695, USA

[3]Lead Contact

*Correspondence: xubowei2004@iccas.ac.cn (B.X.), hjhzlz@iccas.ac.cn (J.H.)

https://doi.org/10.1016/j.joule.2018.10.024

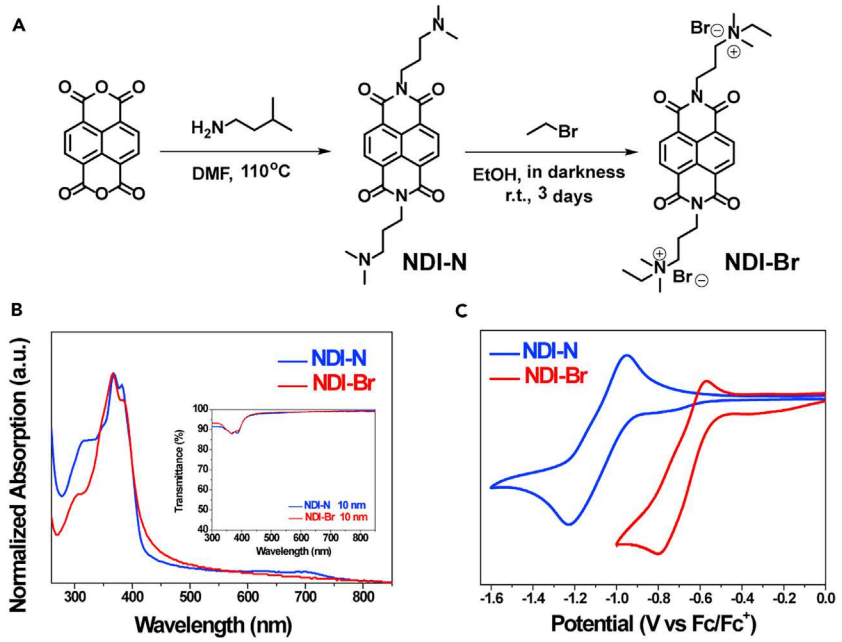

Figure 1. Chemical Synthesis and Photophysical Characterizations

(A) Synthetic route of NDI-N and NDI-Br.

(B) Normalized UV-vis absorption spectra of NDI-N and NDI-Br films. The inset is their transmittance spectra.

(C) Cyclic voltammograms of NDI-N and NDI-Br films on glassy carbon electrodes in 0.1 M Bu_4NPF_6 in acetonitrile solution at a scan of 20 mV/s.

the absorption spectra of NDI-N and NDI-Br as solid films, and the inset provides their transmittance spectra. The absorption maxima at 368 nm are ascribed to the π-π* transition of the NDI unit, while the broad absorption tails from 450 to 750 nm can be assigned to the polaronic transition ($\lambda_{polaron}$), indicating the self-doping effect of the two compounds. Moreover, the high transmittance (over 98%) of the NDI-N and NDI-Br films in the long-wavelength region from 450 to 800 nm avoids the negative effect on the light-harvesting of photoactive layers. Cyclic voltammetry measurements were conducted to evaluate the molecular energy levels of NDI-N and NDI-Br. On the basis of the onset reduction potentials, the lowest unoccupied molecular orbital (LUMO) levels of NDI-N and NDI-Br were determined to be −3.98 and −3.69 eV, respectively (Figure 1C). The low-lying LUMO level of NDI-N is favorable to the electron extraction and transport of CILs. As reported in previous studies, when the LUMO level of CIL is lower than that of the acceptor, a charge can be injected into the CIL without energy barrier and subsequently be transported within the CIL film.[33] In this case, a large thickness window of CIL can be applied to achieve high OSC performances, which is one of critical requirements for the CIL to be processed by printing methods.

Crystallinity and molecular arrangement have important influences on the electron-transport properties of organic semiconductors. We first utilized single-crystal X-ray analysis to investigate the effect of molecular packing on the charge-transport property of NDI-N, as shown in Figures 2A and 2B. There are two molecules per unit cell in the $P\bar{1}$ space group, and each molecule is located on an inversion center. The NDI-N molecules in the lattice exhibit a tilted parallel π-stacking arrangement, and the distances between the packing layers are 3.3 Å. The intermolecular π-π packing distance of NDI-N is among the shortest π-planar distances of NDI-based

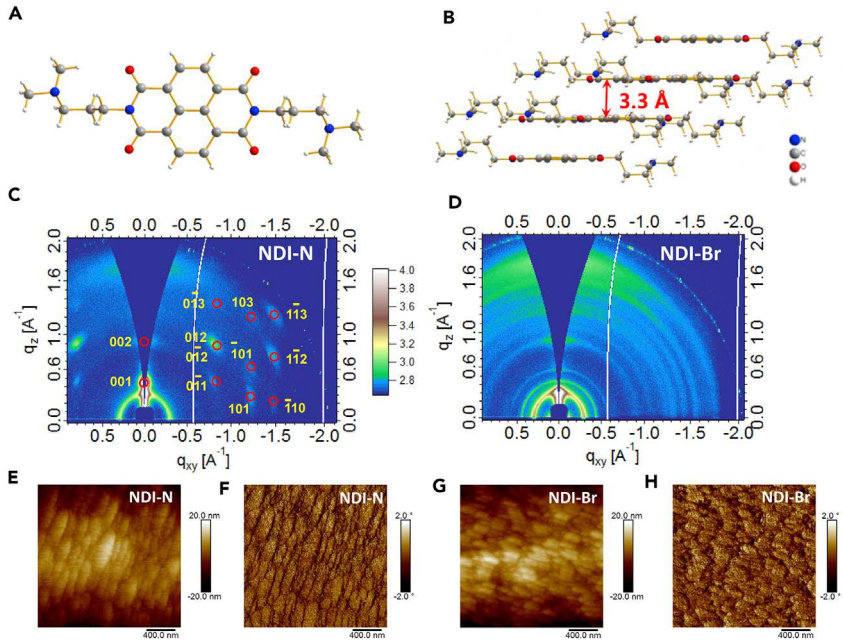

Figure 2. Crystal Structures and Film-Forming Properties of NDI-Based Molecules

(A) Molecular structure of NDI-N.

(B) Crystal π-stacking view of NDI-N.

(C and D) 2D GIWAXS patterns for NDI-N (C) and NDI-Br films deposited on the photoactive layer (D). The incident angle (0.08°) is well below the critical angle (~0.13°) of the PBDB-T-2F:IT-4F blend film.

(E–H) AFM topography (E and G) and phase images (F and H) of NDI-N and NDI-Br films deposited on the photoactive layer.

molecules reported previously.[34–37] The compact π-planar packing of NDI-N is beneficial for enhancing the charge transport. Moreover, grazing-incidence wide-angle X-ray scattering (GIWAXS)[38] was used to measure the neat NDI-N and NDI-Br films deposited on silicon substrates. As can be seen from Figure S2, the NDI-N film exhibits well-defined and pronounced diffraction spots, indicating a high degree of crystalline order. By contrast, the NDI-Br film showed only some weak and irregular diffraction spots, implying a less ordered nature of the film. To probe the actual microstructure of these interlayers in OSC devices, we further studied the NDI-N and NDI-Br films deposited on the photoactive layer by gradually increasing the incident angle from 0.05° to 0.20°. The angle dependence of these samples is shown in Figures S3 and S4. Figures 2C and 2D respectively present the 2D GIWAXS patterns of NDI-N and NDI-Br films deposited on the top of the photoactive layer with a small incident angle of 0.08°, which yield a consistent trend that NDI-N is much more ordered than NDI-Br. By combination with single-crystal X-ray analysis, all the diffraction peaks in the 2D GIWAXS pattern have been indexed,[39] and the (001) plan can be defined as parallel orientation to the substrate. The mean size of the crystallites was acquired through calculating the crystal coherence length (CCL) using the Scherrer equation. The CCL of NDI-N was 10.4 nm, indicating a high ordering of the NDI-N film. As reported in previous works, the highly crystalline molecules tend to aggregate during the film fabrication, resulting in a coarse film surface with numerous pinholes; this not only severely deteriorates the device performance but also brings difficulties in processing CILs. However, as shown in Figures 2E and 2F, the atomic force microscopy (AFM) images of the NDI-N film deposited on the photoactive layer exhibit a smooth and uniform surface with a low root-mean-square roughness (R_q) value of 4.23 nm, indicating that the highly crystalline NDI-N can also

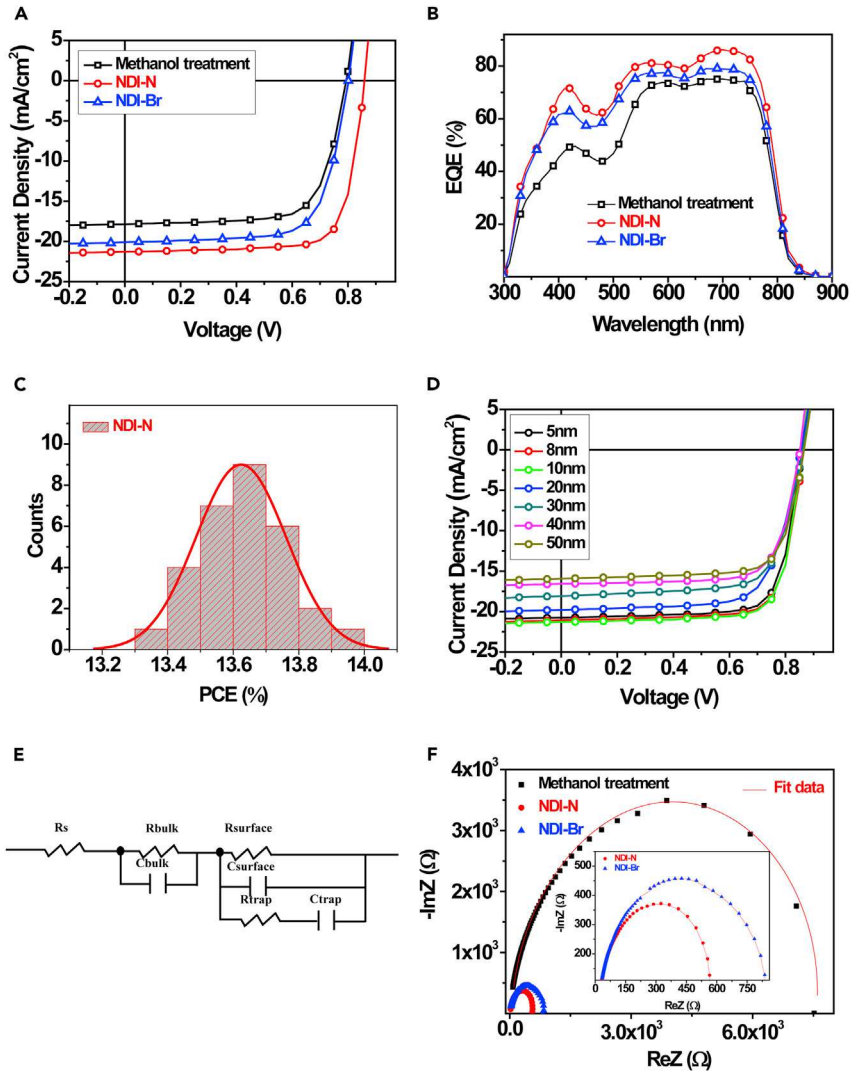

Figure 3. Photovoltaic Parameters of Devices and Electrochemical Impedance Spectroscopy

(A and B) *J-V* (A) and EQE (B) curves of the best-performing NDI-N and NDI-Br-based devices.

(C) Histograms of the PCE counts for 30 individual NDI-N-based cells.

(D) *J-V* curves of the OSC devices with various NDI-N thicknesses.

(E) The equivalent-circuit model employed for EIS fitting of the devices.

(F) Nyquist plots of different CIL film-modified devices.

form desirable films. Based on these results, it can be suggested that the high crystallinity and compact molecular packing is beneficial in improving the electron-transport properties of NDI-N which, in combination with good film-forming property, is the key factor for NDI-N to be processed by printing methods.

To evaluate the performance of the NDI-based compounds as CILs in OSCs, we fabricated conventional devices with the configuration of indium tin oxide (ITO)/poly(3,4-ethylenedioxythiophene) polystyrene sulfonate (PEDOT:PSS)/photoactive layer/NDI-based CIL/Al. Here, a blend based on a polymer donor, PBDB-T-2F, and a non-fullerene acceptor, IT-4F, is used as the photoactive material. For comparison, devices with PFN-Br, ZnO nanoparticles (NPs), and methanol treatment were also fabricated as a control. The current density-voltage (*J-V*) characteristics of the devices and relevant parameters are shown in Figure 3A and Table 1, respectively,

Table 1. Photovoltaic Parameters of Conventional Devices with NDI-N, NDI-Br, and Methanol Treatment and Inverted Device with NDI-N under the Illumination of AM 1.5G, 100 mW cm^{-2}

Devices	V_{oc} (V)	J_{sc} (mA/cm^2)	FF	PCE (%)	J_{cal}[a] (mA/cm^2)	R_s (Ω cm^2)	R_{sh} (kΩ cm^2)
Methanol treatment	0.79	17.9	0.71	10.1	17.3	5.39	1.23
NDI-N	0.86	21.3	0.76	13.9	20.6	2.66	1.85
NDI-Br	0.80	20.1	0.71	11.5	19.4	3.77	0.74
Inverted device (NDI-N)	0.83	21.5	0.71	12.6	20.8	3.53	1.46

[a]Integrated J_{cal} from the EQE curves.

with the external quantum efficiency (EQE) curves displayed in Figure 3B. The optimal thickness was found to be 10 nm for both NDI-N and NDI-Br. The OSC device modified by NDI-N delivered the best PCE of 13.9%, along with a short-circuit current density (J_{sc}) of 21.3 mA/cm^2, an open-circuit voltage (V_{oc}) of 0.86 V, and a fill factor (FF) of 0.76, which is higher than that of the PBDB-T-2F:IT-4F-based device in the most recent report using PFN-Br.[40] Figure 3C presents a PCE histogram of 30 NDI-N-modified devices; over 60% of the devices exhibit PCE values exceeding 13.6%, indicating the good reproducibility of the NDI-N-modified OSCs. For the devices with PFN-Br, ZnO NPs, NDI-Br, and methanol treatment, the PCEs of the devices are 13.5%, 13.1%, 11.5%, and 10.1%, respectively. Electrochemical impedance spectroscopy (EIS) measurements were performed to examine the interface resistance of the devices. Figure 3F shows Nyquist plots of NDI-N-modified devices in the dark. A bias voltage equal to V_{oc} was applied to dissipate the total current.[41] The data were fitted using the equivalent-circuit model from a previous report,[42] and the corresponding results are listed in Table S4. The surface resistance ($R_{surface}$) of the devices with NDI-N, NDI-Br, PFN-Br, ZnO NPs, and methanol treatment was estimated to be 586.6, 884.2, 359.3, 751.8, and 6,475 Ω, respectively. The $R_{surface}$ of fullerene-free devices can be significantly decreased by using NDI-N CILs, indicating the reduced charge recombination and improved charge extraction in the NDI-N-modified OSCs. The stability of devices modified with NDI-N, NDI-Br, PFN-Br, and ZnO NPs was tested under ambient conditions (Figure S9). PCEs of devices modified with NDI-N, NDI-Br, and PFN-Br CILs can retain 83%, 83%, and 86% of their initial PCE values after 20 days, respectively, whereas the PCE of ZnO NPs-modified device declines to 38% of its initial value.

Furthermore, NDI-N was employed for modifying other efficient active layers, including PBDB-T:ITIC, DRTB-T:IDIC, and PBDB-T:IT-M. The *J-V* curves of these devices are provided in Figure S10, and the corresponding photovoltaic parameters are summarized in Table 2. All the devices exhibited PCEs comparable with their highest values in related reports,[43–45] indicating that NDI-N is a universal and effective CIL for various active layers. Moreover, due to its high transparency, NDI-N was used to fabricate inverted devices with a configuration of ITO/NDI-N/PBDB-T-2F:IT-4F/MoO_3/Al, whereby a PCE of 12.6% was achieved (Figure S11 and Table 1). These results suggest that NDI-N is a promising CIL material for various applications in OSCs. We further investigated the effect of NDI-N and NDI-Br thicknesses on the OSC performances. As shown in Figure 3D and Table S2, NDI-N exhibits an outstanding tolerance to thickness variation in fabricating OSCs; i.e., when the NDI-N thickness changed from 5 to 30 nm, the PCE remained at over 11.6%. It is worth noting that the R_s remains almost unchanged and the FF maintains a high value of 0.74 when the NDI-N thickness increases to 50 nm, indicating the excellent electron-transport and collection properties of NDI-N. The excellent thickness

Table 2. Photovoltaic Parameters of Devices Based on NDI-N Films with Different Photoactive Layers

Active Layer	CIL	V_{oc} (V)	J_{sc} (mA/cm^2)	FF	PCE (%)	J_{cal}[a] (mA/cm^2)
PBDB-T:ITIC	NDI-N	0.90	17.4	0.69	10.9	16.1
	NDI-Br	0.84	17.0	0.62	8.87	15.8
PBDB-T:IT-M	NDI-N	0.94	16.9	0.71	11.3	16.1
	NDI-Br	0.88	16.4	0.64	9.29	15.1
DRTB-T:IDIC	NDI-N	0.98	15.5	0.60	9.10	15.3
	NDI-Br	0.94	14.8	0.53	7.44	14.6

[a]Integrated J_{cal} from the EQE curves.

insensitivity of NDI-N for modifying OSCs is crucial for processing the CIL by printing methods. In contrast, the PCEs of the devices modified by NDI-Br, ZnO NPs, and PFN-Br dramatically decreased to 5.20%, 7.88%, and 4.08%, respectively, as the CIL thickness increased to 30 nm (Figure S7 and Table S3).

In an OSC device, the CIL contacts either the electron donor or the electron acceptor at the photoactive layer/CIL interface; therefore, an ideal CIL can extract electrons from both the donor and the acceptor. In previous works, the doping interaction between CILs and PCBM ([6,6]-phenyl-C_{61}-butyric acid methyl ester) has been proved to facilitate the electron extraction of fullerene-based devices;[46] however, doping on non-fullerene acceptors has not yet been reported. Here, electron spin resonance (ESR) spectroscopy was performed to investigate the doping effects of NDI-based molecules. First, the self-doping effect of the NDI-based small molecules can be confirmed by the ESR signals related to delocalized polarons that are observed in the neat NDI-N and NDI-Br films (Figure 4A), which is consistent with the results of UV-visible (UV-vis) absorptions. Second, a much stronger resonance peak with g values of 31.16 is detected in the NDI-N:IT-4F blend, confirming that the non-fullerene acceptor IT-4F can be effectively doped by NDI-N. In contrast, only a moderate ESR signal was observed in the NDI-Br:IT-4F blend because of the self-doping behavior of NDI-Br, suggesting that the doping effect of NDI-Br on IT-4F could be excluded. Lewis basicity can be used to elucidate the different n-doping behaviors of the two blends.[47] Compared with Br^-, the Lewis basicity of the amine group is much stronger, and thus the electron transfer from NDI-N to IT-4F is more efficient, resulting in significant n-doping of IT-4F. As a result, the electron transfer from NDI-N to IT-4F may induce an interfacial dipole layer at the IT-4F/NDI-N interface (Figure 4B), which facilitates electron extraction from the active layer to the cathode.

To verify the above inference, we fabricated electron-only devices with the configuration ITO/ZnO/IT-4F/NDI-N or NDI-Br/Al. Under a reverse bias voltage ranging from −2 to 0 V, at which electrons were injected from ITO and collected by the Al electrode, the current density of the NDI-N-based device is 6-fold higher than that of the NDI-Br-based device (Figure 4C), suggesting that doping on non-fullerene acceptor can facilitate the electron extraction at the photoactive layer/CIL interface. Moreover, doping on the non-fullerene acceptor could effectively improve the rectification characteristic of the device, which was demonstrated by fabricating p-n junction diodes with a structure of ITO/PEDOT:PSS/IT-4F/NDI-based compound (20 nm)/Al and measuring the J-V characteristics in the dark. As shown in Figure S13, the rectification ratio (the quotient of the current density at ±2 V) of the NDI-N-based diode is three times higher than that of the NDI-Br-based device, suggesting that the rectification characteristic of OSC devices can be effectively enhanced by doping the non-fullerene acceptor.

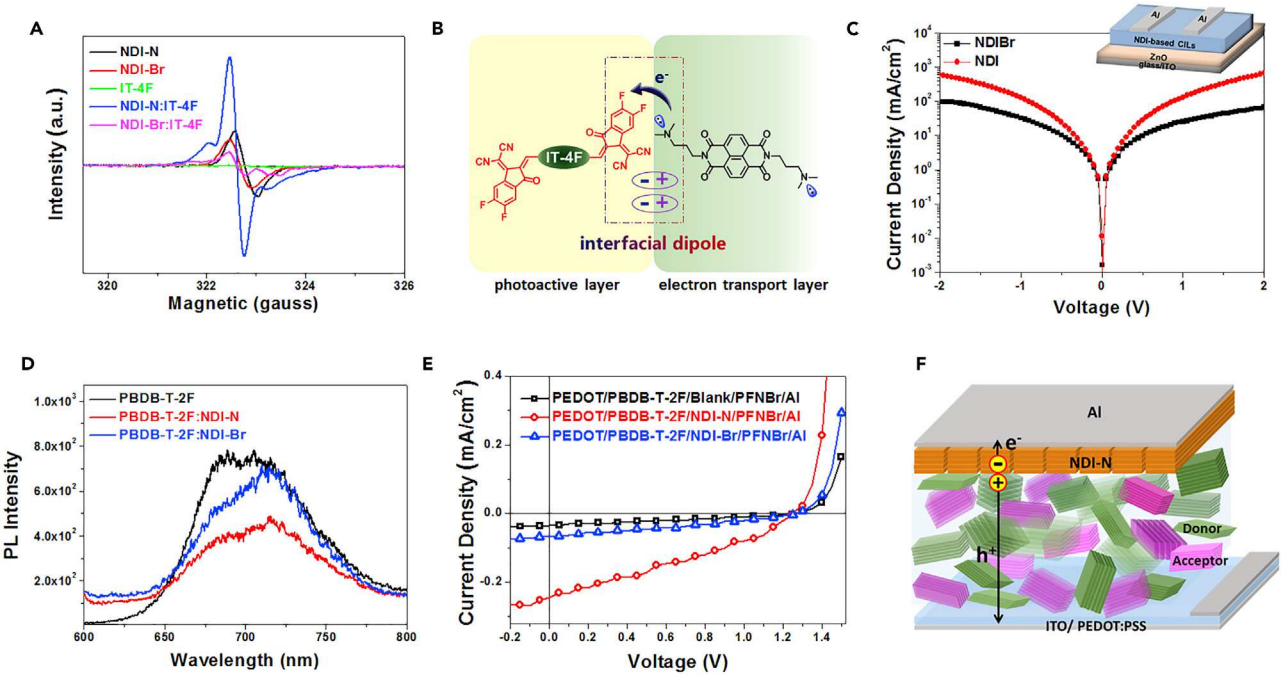

Figure 4. Characterizations of the Electron Extraction Capacity of NDI-N

(A) ESR spectra of the solid samples of NDI-N, NDI-Br, IT-4F, NDI-N:IT-4F, and NDI-Br:IT-4F.

(B) Schematic illustration of interfacial dipole formed by the doping between IT-4F and NDI-N.

(C) Semilogarithmic current density versus voltage characteristics of electron-only devices.

(D) PL spectra of PBDB-T-2F, PBDB-T-2F:NDI-N, and PBDB-T-2F:NDI-Br films.

(E) *J-V* curves of the bilayer heterojunction devices.

(F) Schematic illustration of exciton dissociation at the donor/NDI-N interface.

Furthermore, NDI-N can also extract electrons from polymer donors at the photoactive layer/CIL interface. As shown in Figure 4D, the photoluminescence (PL) emission (under excitation at 680 nm) of PBDB-T-2F was considerably quenched by NDI-N, whereas there was only a slight drop in the PL peak for the PBDB-T-2F:NDI-Br blend. The LUMO level of NDI-N is lower than that of PBDB-T-2F, which induces exciton dissociation at the contact interface between NDI-N and PBDB-T-2F (Figure S5). This result indicates that NDI-N can be used as an electron acceptor in devices. To demonstrate the contribution of NDI-N serving as electron acceptor to photocurrent generation, we fabricated bilayer devices with a configuration of ITO/PEDOT:PSS/PBDB-T-2F/NDI-N or NDI-Br/PFN-Br/Al. As shown in Figure 4E and Table S6, the PBDB-T-2F/NDI-N-based bilayer device showed an improved J_{sc} and an observable photovoltaic effect, suggesting that NDI-N can act as an electron acceptor under illumination. Based on these results, it can be concluded that in contrast to NDI-Br, NDI-N can efficiently extract electrons from both the polymer donor and the non-fullerene acceptor.

To demonstrate the compatibility of the CIL with printing techniques, we processed NDI-N by blade-coating to fabricate large-area OSCs (Figure 5A). The device architecture is the same as that used in the spin-coated devices, and the 1-cm^2 OSCs with ZnO NPs and PFN-Br CILs were also fabricated for comparison. As shown in Figure S15, a large-area NDI-N film of 1 cm^2 (1 cm × 1 cm) was fabricated through a blade-coating approach, and the AFM images of the NDI-N film were collected at different spots along the diagonal line of the film. All the collected AFM images exhibited smooth surfaces with low R_q values of about 2.2 nm, suggesting that the

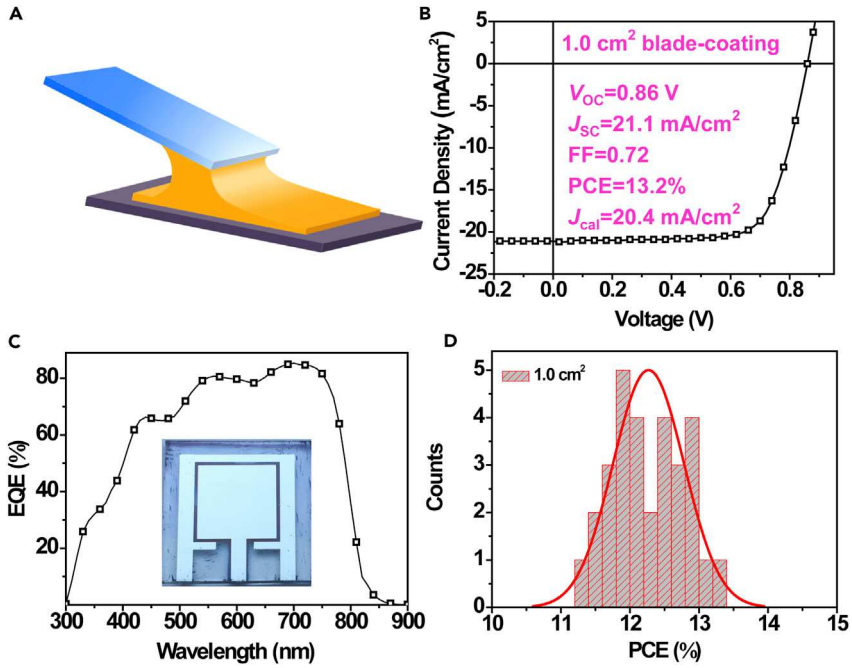

Figure 5. Fabrication and Device Performance of Large-Area OSCs

(A) Schematic illustration of blade-coating processes.

(B and C) *J-V* (B) and EQE (C) curves of devices using blade-coated NDI-N as CIL.

(D) Histograms of the PCE counts for 30 individual 1.0-cm^2 cells.

whole NDI-N film is smooth and uniform. The good wetting property of NDI-N methanol solution on the hydrophobic surface is favorable for making smooth and uniform CIL when printing the CIL on photoactive layers. As shown in Figure S16, the methanol solution drop was immediately spread with the contact angle close to 0° when it contacted the PBDB-T-2F:IT-4F surface, indicating the complete wetting of NDI-N solution on the photoactive layer. The good film-forming properties in combination with the excellent electron transport are favorable for processing NDI-N through printing methods. As shown in Figure 5B, the large-area OSC device of 1 cm^2 with the NDI-N CIL processed by the blade-coating exhibits an outstanding PCE of 13.2%. To the best of our knowledge, this is the highest efficiency reported thus far for large-area OSCs. The photovoltaic performance of the 0.81-cm^2 OSC (0.9 cm × 0.9 cm mask) was certified by the National Institute of Metrology (NIM), and a certified PCE of 12.20% was acquired (Figure S24). It is understandable that the lower PCE certified by the NIM is mainly derived from the slightly decreased J_{sc}. The J_{sc} in the certification is measured with the mask, which is lower than that of the unmasked case due to the non-negligible mask thickness compared with the aperture size. Figure 5D and Table S9 present a PCE histogram of 30 independent cells, in which more than 63% of the cells exhibited PCE values exceeding 12%. To make a comparison with the recent results of large-area devices, we carried out a survey (see Table 3) of state-of-the-art OSCs to date with an area of ca. 1 cm^2. Consequently, the PCE achieved in our work is the highest efficiency at present for large-area OSCs. Moreover, it is worth noting that the NDI-N thickness has little influence on PCEs of large-area devices. When the NDI-N concentration used in the blade-coating was increased from 0.1 to 1.0 mg/mL, the OSC with a thick NDI-N film only showed a moderate decline in PCE (Figure S17 and Table S10). In contrast, when the PFN-Br concentration changed from 0.1 to 1.0 mg/mL, the PCE of the device dramatically decreased from 5.76% to 4.09%. Compared with PFN-Br, the

Table 3. Survey of Photovoltaic Parameters of the State-of-the-Art Large-Area OSCs by Blade-Coating Techniques

Photoactive Layer	Device Area (cm^2)	PCE (%)	Year	Reference
PCDTBT:$PC_{71}BM$	0.64	4.9	2014	Smith et al.[48]
BDTT-S-TR:$PC_{71}BM$	1.44	6.7	2015	Cui et al.[49]
P3HT:$PC_{61}BM$	0.96	2.8	2015	Ye et al.[50]
PTZ1:IDIC	0.81	10.5	2017	Guo et al.[51]
PB-3T:IT-M	1.00	10.1	2018	Kang et al.[12]
PBTA-TF:IT-M	1.00	10.6	2018	Zhao et al.[11]
FTAZ:IT-M	0.56	9.8	2018	Ye et al.[3]
PBDB-T-2F:IT-4F	1.00	12.3 ± 0.9	2018	this work

superior electron transport of NDI-N is favorable for efficient electron collection when the thick NDI-N film is used. Moreover, ZnO NPs also exhibited considerable thickness sensibility in fabricating a 1-cm^2 device (Figure S18 and Table S10). AFM images showed that the thick ZnO NPs film exhibited a non-uniform surface with a high R_q of 5.39 nm, causing a large number of interfacial defects and reducing the FF of the device. Consequently, the large-area device with blade-coated ZnO NPs CILs only exhibits relatively low PCE of 8.89%.

The R_s (5.54 Ω cm^2) of 1-cm^2 OSCs is larger than that of the small-area device (2.66 Ω cm^2), which is indeed responsible for the slight decrease of J_{sc} and FF in the large-area device, while the R_{sh} for the large-area device (2.10 kΩ cm^2) is similar to that of the small-area device (1.85 Ω cm^2). Figure S19 presents the *J-V* characteristic of the large-area device in darkness. The current-leakage of 1-cm^2 OSC has no obvious increase as compared with the small-area device, which may explain the high FF in the large-area device. The small current-leakage implies that the interfacial defects can be suppressed in the large-area device by using the NDI-N CIL. To demonstrate the capacity of NDI-N in passivating defects or pinholes, we fabricated devices with the structure of ITO/PEDOT:PSS/NDI-N or PFN-Br/Al. As shown in Figure S20, the bilayer device with NDI-N exhibits a typical diode characteristic, suggesting that the contact point can still maintain a rectifying property for a selective charge collection even though NDI-N fills the pinholes in the photoactive layer and directly contacts the PEDOT:PSS. On the contrary, the PFN-Br-based device exhibits a linear *J-V* characteristic, implying that the defects or pinholes filled with PFN-Br only have non-selective charge transport. These results suggest that NDI-N can passivate defects or pinholes in photoactive layers, endowing the large-area device with high efficiency.

Conclusions

In conclusion, we reported an *n*-type NDI-based small-molecular semiconductor, NDI-N, as a printable CIL for high-performance OSCs. NDI-N exhibits a unique advantage of combining the merits of high crystallinity and good film-forming properties in one material, endowing the semiconductor with excellent electron-transport properties and good processability. By comparison of NDI-N with NDI-Br, we found that NDI-N can efficiently extract electrons from both the non-fullerene acceptor and the polymer donor. Due to the excellent electron transport and good processability, NDI-N can be processed by a printing method to make large-area devices; i.e., a large-area OSC device of 1 cm^2 was fabricated by using the blade-coated NDI-N CIL and an outstanding PCE of 13.2% was achieved. To the best of our knowledge, this is the highest efficiency thus far for large-area

OSCs. This work not only develops a small molecule with combined merits of high crystallinity and good film-forming properties, but also demonstrates a successful example of processing the CIL by a printing method for making large-area and high-performance OSC devices, which is of great significance for low-cost mass production of OSCs.

EXPERIMENTAL PROCEDURES

Full experimental procedures are provided in the Supplemental Information.

SUPPLEMENTAL INFORMATION

Supplemental Information includes Supplemental Experimental Procedures, 24 figures, and 10 tables and can be found with this article online at https://doi.org/10.1016/j.joule.2018.10.024.

ACKNOWLEDGMENTS

The authors acknowledge the financial support from the NSFC (21504095, 51373181) and the Chinese Academy of Science (XDB12030200, KJZD-EW-J01). L.Y. and H.A. were supported by the US Office of Naval Research (grant ONR, no. N000141712204). S.J.S. was supported by the National Science Foundation under grant no. DGE-1633587. Use of the beamline 7.3.3, Advanced Light Source was supported by the Director of the Office of Science, Office of Basic Energy Sciences, of the US Department of Energy under contract no. DE-AC02-05CH11231.

AUTHOR CONTRIBUTIONS

B.X. and J.H. proposed the research, directed the study, and analyzed the data. Q.K. carried out the device fabrication and characterizations. C.A. helped with X-ray single-crystal analysis. L.Y. and H.A. performed GIWAXS measurements. S.J.S. indexed the diffraction peaks in the GIWAXS measurements. H.Y. and S.Z. provided the photovoltaic materials. B.X., J.H., and Q.K. prepared the manuscript. B.X. and J.H. supervised the whole project. All authors discussed the results and commented on the manuscript.

DECLARATION OF INTERESTS

The authors declare no competing interests.

Received: August 30, 2018
Revised: October 12, 2018
Accepted: October 22, 2018
Published: November 15, 2018

REFERENCES

1. Heeger, A.J. (2014). 25th anniversary article: bulk heterojunction solar cells: understanding the mechanism of operation. Adv. Mater. *26*, 10–27.

2. Yu, G., Gao, J., Hummelen, J.C., Wudl, F., and Heeger, A.J. (1995). Polymer photovoltaic cells—enhanced efficiencies via a network of internal donor-acceptor heterojunctions. Science *270*, 1789–1791.

3. Ye, L., Xiong, Y., Zhang, Q., Li, S., Wang, C., Jiang, Z., Hou, J., You, W., and Ade, H. (2018). Surpassing 10% efficiency benchmark for nonfullerene organic solar cells by scalable coating in air from single nonhalogenated solvent. Adv. Mater. *30*, 1705485.

4. Song, W., Fan, X., Xu, B., Yan, F., Cui, H., Wei, Q., Peng, R., Hong, L., Huang, J., and Ge, Z. (2018). All-solution-processed metal-oxide-free flexible organic solar cells with over 10% efficiency. Adv. Mater. *30*, 1800075.

5. Diao, Y., Zhou, Y., Kurosawa, T., Shaw, L., Wang, C., Park, S., Guo, Y., Reinspach, J.A., Gu, K., Gu, X., et al. (2015). Flow-enhanced solution printing of all-polymer solar cells. Nat. Commun. *6*, 7955.

6. Zhang, S., Qin, Y., Zhu, J., and Hou, J. (2018). Over 14% efficiency in polymer solar cells enabled by a chlorinated polymer donor. Adv. Mater. *30*, 1800868.

7. Li, S., Ye, L., Zhao, W., Yan, H., Yang, B., Liu, D., Li, W., Ade, H., and Hou, J. (2018). A wide band gap polymer with a deep highest occupied molecular orbital level enables 14.2% efficiency in polymer solar cells. J. Am. Chem. Soc. *140*, 7159–7167.

8. Strohm, S., Machui, F., Langner, S., Kubis, P., Gasparini, N., Salvador, M., McCulloch, I., Egelhaaf, H.J., and Brabec, C.J. (2018). P3HT:

non-fullerene acceptor based large area, semi-transparent PV modules with power conversion efficiencies of 5%, processed by industrially scalable methods. Energy Environ. Sci. *11*, 2225–2234.

9. Søndergaard, R., Hösel, M., Angmo, D., Larsen-Olsen, T.T., and Krebs, F.C. (2012). Roll-to-roll fabrication of polymer solar cells. Mater. Today *15*, 36–49.

10. Sandstrom, A., Dam, H.F., Krebs, F.C., and Edman, L. (2012). Ambient fabrication of flexible and large-area organic light-emitting devices using slot-die coating. Nat. Commun. *3*, 1002.

11. Zhao, W., Zhang, S., Zhang, Y., Li, S., Liu, X., He, C., Zheng, Z., and Hou, J. (2018). Environmentally friendly solvent-processed organic solar cells that are highly efficient and adaptable for the blade-coating method. Adv. Mater. *30*, 1704837.

12. Kang, Q., Yang, B., Xu, Y., Xu, B., and Hou, J. (2018). Printable MoO_x anode interlayers for organic solar cells. Adv. Mater. *30*, 1801718.

13. He, Z.C., Zhong, C.M., Huang, X., Wong, W.Y., Wu, H.B., Chen, L.W., Su, S.J., and Cao, Y. (2011). Simultaneous enhancement of open-circuit voltage, short-circuit current density, and fill factor in polymer solar cells. Adv. Mater. *23*, 4636–4643.

14. Lv, M.L., Li, S.S., Jasieniak, J.J., Hou, J.H., Zhu, J., Tan, Z.A., Watkins, S.E., Li, Y.F., and Chen, X.W. (2013). A hyperbranched conjugated polymer as the cathode interlayer for high-performance polymer solar cells. Adv. Mater. *25*, 6889–6894.

15. Liu, S.J., Zhang, K., Lu, J.M., Zhang, J., Yip, H.L., Huang, F., and Cao, Y. (2013). High-efficiency polymer solar cells via the incorporation of an amino-functionalized conjugated metallopolymer as a cathode interlayer. J. Am. Chem. Soc. *135*, 15326–15329.

16. Lin, Y., Jin, Y., Dong, S., Zheng, W., Yang, J., Liu, A., Liu, F., Jiang, Y., Russell, T.P., Zhang, F., et al. (2018). Printed nonfullerene organic solar cells with the highest efficiency of 9.5%. Adv. Energy Mater. *8*, 1701942.

17. Gao, L., Zhang, Z.G., Xue, L., Min, J., Zhang, J., Wei, Z., and Li, Y. (2016). All-polymer solar cells based on absorption-complementary polymer donor and acceptor with high power conversion efficiency of 8.27%. Adv. Mater. *28*, 1884–1890.

18. Sun, D., Meng, D., Cai, Y., Fan, B., Li, Y., Jiang, W., Huo, L., Sun, Y., and Wang, Z. (2015). Non-fullerene-acceptor-based bulk-heterojunction organic solar cells with efficiency over 7. J. Am. Chem. Soc. *137*, 11156–11162.

19. Zhang, Z.-G., Qi, B., Jin, Z., Chi, D., Qi, Z., Li, Y., and Wang, J. (2014). Perylene diimides: a thickness-insensitive cathode interlayer for high performance polymer solar cells. Energy Environ. Sci. *7*, 1966–1973.

20. Liu, Y., Cole, M.D., Jiang, Y., Kim, P.Y., Nordlund, D., Emrick, T., and Russell, T.P. (2018). Chemical and morphological control of interfacial self-doping for efficient organic electronics. Adv. Mater. *30*, 1705976.

21. Zhao, K., Ye, L., Zhao, W., Zhang, S., Yao, H., Xu, B., Sun, M., and Hou, J. (2015). Enhanced efficiency of polymer photovoltaic cells via the incorporation of a water-soluble naphthalene diimide derivative as a cathode interlayer. J. Mater. Chem. C *3*, 9565–9571.

22. Jia, T., Sun, C., Xu, R., Chen, Z., Yin, Q., Jin, Y., Yip, H.L., Huang, F., and Cao, Y. (2017). Naphthalene diimide based n-type conjugated polymers as efficient cathode interfacial materials for polymer and perovskite solar cells. ACS Appl. Mater. Interfaces *9*, 36070–36081.

23. Hu, Z., Chen, Z., Zhang, K., Zheng, N., Xie, R., Liu, X., Yang, X., Huang, F., and Cao, Y. (2017). Self-doped n-type water/alcohol soluble-conjugated polymers with tailored backbones and polar groups for highly efficient polymer solar cells. Solar RRL *1*, 1700055.

24. Wu, Z., Sun, C., Dong, S., Jiang, X.-F., Wu, S., Wu, H., Yip, H.-L., Huang, F., and Cao, Y. (2016). n-Type water/alcohol-soluble naphthalene diimide-based conjugated polymers for high-performance polymer solar cells. J. Am. Chem. Soc. *138*, 2004–2013.

25. Guo, X., Wang, X., Zhang, J., Yu, S., Yu, W., Fu, P., Liu, X., Tu, D., and Li, C. (2018). Lowering molecular symmetry to improve morphological property of hole transport layer for stable perovskite solar cells. Angew. Chem. Int. Ed. https://doi.org/10.1002/anie.201807402.

26. Hawash, Z., Ono, L.K., Raga, S.R., Lee, M.V., and Qi, Y. (2015). Air-exposure induced dopant redistribution and energy level shifts in spin-coated Spiro-MeOTAD films. Chem. Mater. *27*, 562–569.

27. Kato, Y., Ono, L.K., Lee, M.V., Wang, S., Raga, S.R., and Qi, Y. (2015). Silver iodide formation in methyl ammonium lead iodide perovskite solar cells with silver top electrodes. Adv. Mater. Interfaces *2*, 1500195.

28. Ono, L.K., Raga, S.R., Remeika, M., Winchester, A.J., Gabe, A., and Qi, Y. (2015). Pinhole-free hole transport layers significantly improve the stability of MAPbI3-based perovskite solar cells under operating conditions. J. Mater. Chem. A *3*, 15451–15456.

29. Wang, Y., Yan, Z., Guo, H., Uddin, M.A., Ling, S., Zhou, X., Su, H., Dai, J., Woo, H.Y., and Guo, X. (2017). Effects of bithiophene imide fusion on the device performance of organic thin-film transistors and all-polymer solar cells. Angew. Chem. Int. Ed. *56*, 15304–15308.

30. Hou, J., Wu, Y., An, C., Shi, L., Yang, L., Qin, Y., Liang, N., He, C., and Wang, Z. (2018). Crucial role of chlorinated thiophene orientation in conjugated polymers for photovoltaic devices. Angew. Chem. Int. Ed. https://doi.org/10.1002/anie.201807865.

31. Jung, S.-K., Heo, J.H., Lee, D.W., Lee, S.-C., Lee, S.-H., Yoon, W., Yun, H., Im, S.H., Kim, J.H., and Kwon, O.P. (2018). Nonfullerene electron transporting material based on naphthalene diimide small molecule for highly stable perovskite solar cells with efficiency exceeding 20%. Adv. Funct. Mater. *28*, 1800346.

32. Huang, F., Wu, H., Wang, D., Yang, W., and Cao, Y. (2004). Novel electroluminescent conjugated polyelectrolytes based on polyfluorene. Chem. Mater. *16*, 708–716.

33. Sun, C., Wu, Z., Hu, Z., Xiao, J., Zhao, W., Li, H.-W., Li, Q.-Y., Tsang, S.-W., Xu, Y.-X., Zhang, K., et al. (2017). Interface design for high-efficiency non-fullerene polymer solar cells. Energy Environ. Sci. *10*, 1784–1791.

34. Zheng, D., Zhang, M., and Zhao, G. (2017). The promotion effects of thionation and isomerization on charge carrier mobility in naphthalene diimide crystals. Phys. Chem. Chem. Phys. *19*, 28175–28181.

35. Lee, W.-Y., Oh, J.H., Suraru, S.-L., Chen, W.-C., Würthner, F., and Bao, Z. (2011). High-mobility air-stable solution-shear-processed n-channel organic transistors based on core-chlorinated naphthalene diimides. Adv. Funct. Mater. *21*, 4173–4181.

36. Matsunaga, Y., Goto, K., Kubono, K., Sako, K., and Shinmyozu, T. (2014). Photoinduced color change and photomechanical effect of naphthalene diimides bearing alkylamine moieties in the solid state. Chem. Eur. J. *20*, 7309–7316.

37. Kao, C.-C., Lin, P., Shen, Y.-Y., Yan, J.-Y., Ho, J.-C., Lee, C.-C., and Chan, L.-H. (2008). Solid-state structure of the naphthalene-based n-type semiconductor, and performance improved with Mo-based source/drain electrodes. Synth. Met. *158*, 299–305.

38. Hexemer, A., Bras, W., Glossinger, J., Schaible, E., Gann, E., Kirian, R., MacDowell, A., Church, M., Rude, B., and Padmore, H. (2010). A SAXS/WAXS/GISAXS beamline with multilayer monochromator. J. Phys. Conf. Ser. *247*, 012007.

39. Smilgies, D.M., and Blasini, D.R. (2007). Indexation scheme for oriented molecular thin films studied with grazing-incidence reciprocal-space mapping. J. Appl. Cryst. *40*, 716–718.

40. Li, W., Ye, L., Li, S., Yao, H., Ade, H., and Hou, J. (2018). A high-efficiency organic solar cell enabled by the strong intramolecular electron push-pull effect of the nonfullerene acceptor. Adv. Mater. *30*, 1707170.

41. Xu, Q., Wang, F.Z., Tan, Z.A., Li, L.J., Li, S.S., Hou, X.L., Sun, G., Tu, X.H., Hou, J.H., and Li, Y.F. (2013). High-performance polymer solar cells with solution-processed and environmentally friendly CuO_x anode buffer layer. ACS Appl. Mater. Interfaces *5*, 10658–10664.

42. Zhou, H., Zhang, Y., Seifter, J., Collins, S.D., Luo, C., Bazan, G.C., Nguyen, T.Q., and Heeger, A.J. (2013). High-efficiency polymer solar cells enhanced by solvent treatment. Adv. Mater. *25*, 1646–1652.

43. Zhao, W., Qian, D., Zhang, S., Li, S., Inganas, O., Gao, F., and Hou, J. (2016). Fullerene-free polymer solar cells with over 11% efficiency and excellent thermal stability. Adv. Mater. *28*, 4734–4739.

44. Li, S., Ye, L., Zhao, W., Zhang, S., Mukherjee, S., Ade, H., and Hou, J. (2016). Energy-level modulation of small-molecule electron acceptors to achieve over 12% efficiency in polymer solar cells. Adv. Mater. *28*, 9423–9429.

45. Zhang, H., Wang, X., Yang, L., Zhang, S., Zhang, Y., He, C., Ma, W., and Hou, J. (2017). Improved domain size and purity enables efficient all-

small-molecule ternary solar cells. Adv. Mater. *29*, 1703777.

46. Li, C.Z., Chueh, C.C., Ding, F.Z., Yip, H.L., Liang, P.W., Li, X.S., and Jen, A.K.Y. (2013). Doping of fullerenes via anion-induced electron transfer and its implication for surfactant facilitated high performance polymer solar cells. Adv. Mater. *25*, 4425–4430.

47. Chen, Z., Hu, Z., Wu, Z., Liu, X., Jin, Y., Xiao, M., Huang, F., and Cao, Y. (2017). Counterion-tunable n-type conjugated polyelectrolytes for the interface engineering of efficient polymer solar cells. J. Mater. Chem. A *5*, 19447–19455.

48. Smith, C., Rhodes, R., Beliatis, M., Jayawardena, K., Rozanski, L., Mills, C., and Silva, S. (2014). Graphene oxide hole transport layers for large area, high efficiency organic solar cells. Appl. Phys. Lett. *105*, 073304.

49. Cui, C., Guo, X., Min, J., Guo, B., Cheng, X., Zhang, M., Brabec, C., and Li, Y. (2015). High-performance organic solar cells based on a small molecule with alkylthio-thienyl-conjugated side chains without extra treatments. Adv. Mater. *27*, 7469–7475.

50. Ye, F., Chen, Z., Zhao, X., Chen, J., and Yang, X. (2015). "Layer-filter threshold" technique for near-infrared laser ablation in organic semiconductor device processing. Adv. Energy Mater. *25*, 4453–4461.

51. Guo, B., Li, W., Guo, X., Meng, X., Ma, W., Zhang, M., and Li, Y. (2017). High efficiency nonfullerene polymer solar cells with thick active layer and large area. Adv. Mater. *29*, 1702291.